Nanocrystalline Mesoporous γ-Alumina Powders "UPMC1 Material" Gathers Thermal and Chemical Stability with High Surface Area

Cédric Boissière,[†] Lionel Nicole,[†] Christelle Gervais,[†] Florence Babonneau,[†] Markus Antonietti,[‡] Heinz Amenitsch,[§] Clément Sanchez,[†] and David Grosso*[,†]

Chimie de la Matière Condensée de Paris, UMR UPMC-CNRS 7574, Université Pierre et Marie Curie (Paris 6), 4 place Jussieu, Tour 54-5E, 75252 Paris 05, France, Max Planck Institute of Colloids and Interfaces, Research Campus Golm, D-14424 Potsdam, Germany, Institute of Biophysics and X-ray Structure Research, Austrian Academy of Sciences, Steyrergasse 17/VI, 8010 Graz, Austria

Received June 27, 2006. Revised Manuscript Received July 20, 2006

The designed elaboration of alumina sub-micrometric spherical powder that combines 3D ordered mesoporosity of high accessibility, nanocrystalline structure, and thermal stability up to 900 °C is reported. The strategy used to elaborate such new materials labeled "UPMC1" involves specific block-copolymer templating, aluminum sol−gel chemistry, tuned aerosol generation (spray drying), and sequential thermal treatments that allow designing of a whole set of mesoporous catalytic supports by adjusting ceramization conditions between 700 and 900 °C. When calcination temperature reaches 700 °C, the network remains amorphous and displays structural features of highly porous materials (i.e., porosity, 0.56 $cm^3 \cdot g^{-1}$; surface area, 403 $m^2 \cdot g^{-1}$; well-calibrated pore diameter, 13 nm). After 30 min at 900 °C, crystallization into γ-Al_2O_3 particles of around 6 nm has occurred, which has modified the network characteristics (i.e., porosity, 0.34 $cm^3 \cdot g^{-1}$; surface area, 134 $m^2 \cdot g^{-1}$; well-calibrated pore diameter, 12.5 nm) without destroying the mesostructure. Both amorphous and crystalline final materials present the remarkable properties of mesoporous materials with the unique amphoteric properties of the γ-alumina surface (40% of tetragonal acid sites) that have great potential application in catalysis, in environment, and as an adsorbent. The present work points out that ordered mesoporosity has the ability to stabilize materials with amorphous or metastable crystalline structure at higher temperatures than what is observed for nonordered mesoporous analogous systems. Such a phenomenon is discussed on the basis of extensive materials characterization mainly based on TEM, XRD, and ^{29}Al high-resolution solid-state NMR.

Introduction

Porous ceramic materials are a wide family of compounds that are usually developed around their unique physicochemical properties associated with their high surface area and their high mechanical and thermal stability. Among them, the zeolite types exhibit the highest surface area and the best thermal stability as a result of their well-calibrated micropores created by the association of silicate or aluminosilicate molecular cage building units into crystalline ordered networks. With use of the similar synthesis concept of organic templating, silica and non-silica materials with ordered mesoporosity are nowadays commonly prepared from self-assembly of sol−gel inorganic precursors with surfactants.[1,2] They have been widely studied since their first report by Mobil & Co.[1] and can now be prepared with various porous structures (2D and 3D) and calibrated pore sizes ranging from 2 to 40 nm.[3,4] Ordered mesoporous oxide materials with crystalline networks can be prepared by nanocasting from the previous silica-based materials.[5−8] However, this latter technique requires multistep synthesis that involves impregnation and elimination of the formal silica templates. On the other hand, the direct preparation, from the hybrid mesophase, of ordered and well-defined mesoporosity coexisting with a fully crystalline network, as it is for zeolites, has only been reported for thin films of transition metal oxides,[9−11] perovskite,[12] and alumina[13] and for hybrid silica/aromatic powders, where phenyl bridging

* To whom correspondence should be addressed. Tel.: 33 (0) 1 44 27 55 42. Fax: 33 (0) 1 44 27 47 69. E-mail: grosso@ccr.jussieu.fr.
[†] Université Pierre et Marie Curie (Paris 6).
[‡] Max Planck Institute of Colloids and Interfaces.
[§] Austrian Academy of Sciences.

(1) Kresge, C. T.; Leonowicz, M. E.; Roth, W. J.; Vartuli, J. C.; Beck, J. S. *Nature* **1992**, *359*, 710.
(2) Yang, P.; Zhao, D.; Margolese, D. I.; Chmelka, B. F.; Stucky, G. D. *Nature* **1998**, *583*, 395.
(3) Ciesla, U.; Schuth, F. *Microporous Mesoporous Mater.* **1999**, *27*, 131.
(4) Soler-Illia, G. J. A. A.; Sanchez, C.; Lebeau, B.; Patarin, J. *Chem. Rev.* **2002**, *102*, 4093.
(5) Tian, B.; Liu, X.; Yang, H.; Xie, S.; Yu, C.; Tu, B.; Zhao, D. *Adv. Mater.* **2003**, *15*, 1370.
(6) Dong, A.; Ren, N.; Tang, Y.; Wang, Y.; Zhang, Y.; Hua, W.; Gao, Z. *J. Am. Chem. Soc.* **2003**, *125*, 4976.
(7) Wang, Y.; Yang, C.-M.; Schmidt, W.; Spliethoff, B.; Bill, E.; Schueth, F. *Adv. Mater.* **2005**, *17*, 53.
(8) Laha, S.-C.; Ryoo, R. *Chem. Commun.* **2003**, 2138.
(9) Grosso, D.; Soler Illia, G. J. A. A.; Babonneau, F.; Sanchez, C. *Adv. Mater.* **2001**, *13*, 1085.
(10) Crepaldi, E. L.; Soler-Illia, G. J. A. A.; Grosso, D.; Cagnol, F.; Ribot, F.; Sanchez, C. *J. Am. Chem. Soc.* **2003**, *125*, 9770.
(11) Grosso, D.; Soler-Illia, G. J. A. A.; Crepaldi, E. L.; Cagnol, F.; Sinturel, C.; Bourgeois, A.; Brunet-Bruneau, A.; Amenitsch, H.; Albouy, P. A.; Sanchez, C. *Chem. Mater.* **2003**, *24*, 4562.
(12) Grosso, D.; Boissière, C.; Smarsly, B.; Brezesinski, T.; Pinna, N.; Albouy, P. A.; Amenitsch, H.; Antonietti, M.; Sanchez, C. *Nat. Mater.* **2004**, *3*, 787.

10.1021/cm061489j CCC: $33.50
Published on Web 10/04/2006

groups stack into the walls through π interaction.[14] Nevertheless, the stabilization of pure ceramic class nanocrystalline ordered mesoporous materials under powder form would be a breakthrough in the heterogeneous catalysis area. Many efforts are for instance dedicated to the preparation of TiO_2, CeO_2, or Al_2O_3, for their high catalytic and photocatalytic activity where high surface area, controlled porosity, and nanocrystallinity are simultaneously required.[3]

As a result of its hardness, its hydrolytic stability, its amphoteric character, and its thermal stability, porous alumina (Al_2O_3) is a highly attractive material since it finds applications in ultrafiltration of salts,[15] as an adsorbent in environmental treatment,[16] as a car exhaust catalyst,[17] as a heterogeneous catalysis support for hydrodechlorination,[18,19] and in petroleum refinement.[20] According to the state of the art, ordered mesoporosity has been reported for boehmite,[21] gibbsite,[22,23] and alumina through the template approach[25−31] or without template,[32−34] but also by porogen beads inclusion,[35] by nanocasting within mesoporous carbon networks (CMK),[36] or by anodizing.[15] However, none of these materials combine crystalline pure γ-Al_2O_3, of high thermal stability, with a well-ordered porosity narrowly distributed and adjusted at the mesoscopic scale. The present article describes the preparation of crystalline ordered mesoporous pure Al_2O_3 powders. The latter is synthesized through evaporation-induced self-assembly[37] between $[Al(OH)(H_2O)_5]^{2+}\cdot 2Cl^{-}$ [22] and PB(co-E)-*b*PEO (hydrogenated polybutylene-coethylene-*block*-polyethyleneoxide) block copolymers triggered during an aerosol particle generation process.[38] This UPMC1 material presents the unique combination of alumina properties (robustness, amphoteric, and hydrolytic stability) with the accessibility and high surface area of ordered mesoporous materials. These conclusions are supported through careful structural analyses performed by transmission electron microscopy (TEM), small-angle X-ray scattering (SAXS), N_2-adsorption−desorption, X-ray diffraction (XRD), and ^{27}Al nuclear magnetic resonance (NMR) spectroscopy.

Experimental Section

γ-Alumina mesoporous spheres were prepared by aerosol generation of an initial solution using an ITS (model 3076) atomizer. After being pulverized within dry carrying air, the solution droplets are allowed to dry in a short tube before being fired for a few seconds within an on-line furnace at 400 °C. The resulting powder is then collected on a 0.45 μm mesh filter. The initial solution is prepared by dissolving 3 g of $AlCl_3\cdot 6H_2O$ and 0.6 g of $[E(B)]_{75}$-$[EO]_{86}$ block copolymer (hydrogenated polyethylene-cobutylene-polyethyleneoxide, synthesized at the Max Plank Institute of Colloids and Interfaces, Golm, Germany) into 50 mL of absolute EtOH and 5 mL of H_2O. Then 0.2 mL of 1 M NH_3 is added to the solution, which remains at least 15 days under vigorous stirring before pulverization. The powder is progressively heated under air up to 900 °C with the following steps: 24 h at 100 °C + 12 h at 300 °C + 1 h at 500 °C + 30 min at 700 °C + 10−30 min at 900 °C (ramps: 50 °C·min^{-1} below 500 °C and 5 °C·min^{-1} above 500 °C). Each sample was independently thermally treated before being characterized. ^{27}Al MAS NMR spectra were recorded on a Bruker Avance 400 spectrometer operating at 104.26 MHz with a Bruker high-speed MAS probe head. Samples were spun at 30 kHz using 2.5 mm ZrO_2 rotors. Small pulse flip angles ($<\pi/12$) were applied, thus enabling a linear regime excitation for the spin system.[39] Chemical shifts were referenced to an acidic aqueous solution of $Al(NO_3)_3$ (1 M). The structure of powders was additionally assessed by XRD (Bruker D8: 15 s acquisition every 0.05° in Bragg−Brentano geometry), SAXS (Austrian beam line of Elettra synchrotron, Italy: 10 s exposition), TEM (Jeol 100 CX II), and N_2-adsorption−desorption (asap 2010 Micromeritics).

Results and Discussion

Figure 1 represents TEM images of typical entire particles of γ-Al_2O_3 calcined for 30 min at 700 °C (a) and 30 min at 900 °C (b), representative of all the samples. Particles have spherical shapes and are polydispersed in size (ranging from several tens to several hundreds of nanometers) with an average dimension of 150 nm, which is typical of aerosol-generated particles obtained by evaporation of droplets in these conditions.[40] Both materials reveal well-ordered organization of homogeneous spherical pores, exhibiting an

(13) Kuemmel, M.; Grosso, D.; Boissière, C.; Smarsly, B.; Brezesinski, T.; Albouy, P. A.; Amenitsch, H.; Sanchez, C. *Angew. Chem.* **2005**, *44*, 4589.
(14) Inagaki, S.; Guan, S.; Ohsuma, T.; Terasaki, O. *Nature* **2004**, *416*, 304.
(15) Schaep, J.; Vandecasteele, C.; Peeters, B.; Luyten, J.; Dotremont, C.; Roels, D. *J. Membr. Sci.* **1999**, *163*, 227.
(16) Kim, Y.; Kim, C.; Choi, I.; Rengaraj, S.; Yi, J. *Environ. Sci. Technol.* **2004**, *38*, 924.
(17) Narula, C. K. *Mater. Res. Soc. Symp. Proc.* (*Microporous Macroporous Mater.*) **1996**, *431*, 331.
(18) Euzen, P.; Raybaud, P.; Krokidis, X.; Toulhoat, H.; Le Loader, J.-L.; Jolivet, J.-P.; Froidfond, C. *Handbook of Porous Marerials*; Schuth, F., Sing, K., Weitkamps, J., Eds.; Wiley-VCH: Weinheim, Germany, 2002; Chapter 4.7.2., p 1591.
(19) Kim, P.; Joo, J. B.; Kim, Y.; Kim, C.; Kim, H.; Park, Y.; Lee, J. H.; Song, I. K.; Yi, J. *Catal. Lett.* **2005**, *104*, 181.
(20) Liu, Y.; Zhang, Z.; Hicks, R. W.; Pinnavaia, T. J. *Prepr.-Am. Chem. Soc., Div. Pet. Chem.* **2003**, *48*, 194.
(21) Hicks, R. W.; Pinnavaia, T. J. *Chem. Mater.* **2003**, *15*, 78.
(22) Pidol, L.; Grosso, D.; Soler Illia, G.A.A.; Crepaldi, E.; Albouy, P. A.; Amenitsche, H.; Euzen, P.; Sanchez, C. *J. Mater. Chem.* **2002**, *3*, 557.
(23) Idrissi-Kandri, N.; Ayral, A.; Klotz, M.; Albouy, P.A.; El Mansouri, A.; Van der Lee, A.; Guizard, C. *Mater. Lett.* **2001**, *50*, 57.
(24) Schüth, F. *Chem. Mater.* **2001**, *13*, 3184.
(25) Cejka, J.; Kooyman, P. J.; Vesela, L.; Rathousky, J.; Zukal, A. *Phys. Chem. Chem. Phys.* **2002**, *4*, 4823.
(26) Gonz ález-Peña, V.; Díaz, I.; Márquez-Alvarez, C.; Sastre, E.; Pérez-Pariente, J. *Microporous Mesoporous Mater.* **2001**, *44−45*, 203.
(27) Rana, S.; Ram, S. *Phys. Status Solidi A* **2004**, *201*, 427.
(28) Zhang, X.; Zhang, F.; Chan, K. Y. *Mater. Lett.* **2004**, *58*, 2872.
(29) Cabrera, S.; El Haskouri, J.; Alamo, J.; Beltran, A.; Beltran, D.; Mendioroz, S.; Marcos, M. D.; Amoros, P. *Adv. Mater.* **1999**, *11*, 379.
(30) Zhang, W.; Pinnavaia, T. J. *Chem. Commun.* **1998**, 1185.
(31) Niesz, K.; Yang, P.; Somorjai, G. A. *Chem. Commun.* **2005**, 1986.
(32) Baumann, T. F.; Gash, A. E.; Chinn, S. C.; Sawvel, A. M.; Maxwell, R. S.; Satcher, J. H. *Chem. Mater.* **2005**, *17*, 395.
(33) Macedo, M. I. F.; Osawa, C. C.; Bertran, C. A. *J. Sol-Gel Sci. Technol.* **2004**, *30*, 135.
(34) Vaudri, F.; Khodabandeh, S.; Davis, M. E. *Chem. Mater.* **1996**, *8*, 1451.
(35) Vaudreuil, S.; Bousmina, M.; Kaliaguine, S.; Bonneviot, L. *Microporous Mesoporous Mater.* **2001**, *44−45*, 249.
(36) Lee, J. S.; Joo, S. H.; Ryoo, R. *Stud. Surf. Sci. Catal.* (*Nanotechnology in Mesostructured Materials*) **2003**, *146*, 33.
(37) Grosso, D.; Cagnol, F.; Soler-Illia, G. J. de A. A.; Crepaldi, E. L.; Albouy, P. A.; Amenitch, H.; Brunet-Bruneau, A.; Sanchez, C. *Adv. Funct. Mater.* **2004**, *14*, 309.
(38) Lu, Y.; Fan, H.; Stump, A.; Ward, T. L.; Rieker, T.; Brinker, C. J. *Nature* **1999**, *398*, 223.
(39) Man, P. P. *Mol. Phys.* **1993**, *78*, 307.
(40) Baccile, N.; Grosso, D.; Sanchez, C. *J. Mater. Chem.* **2003**, *13*, 3011.

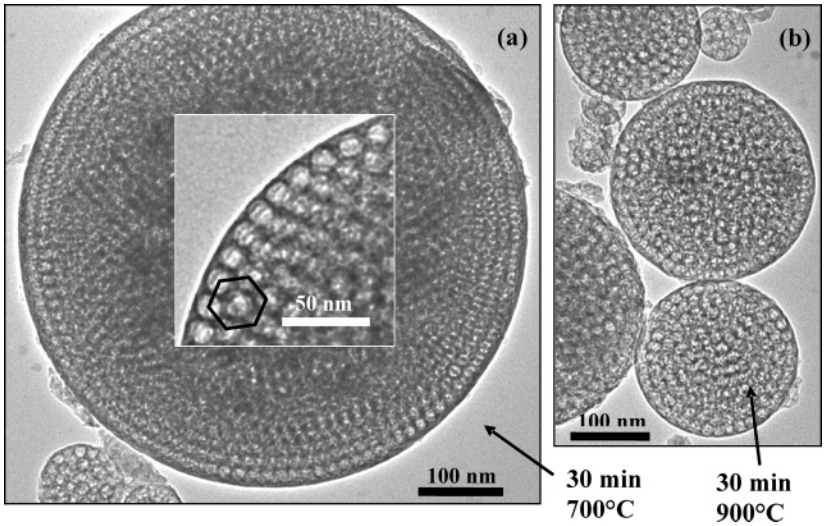

Figure 1. TEM images showing the mesoporous structure of a particle calcined 30 min at 700 °C (a) and 30 min (b) at 900 °C under air. Insert (a): compact arrangement of spherical pores at the particle interface.

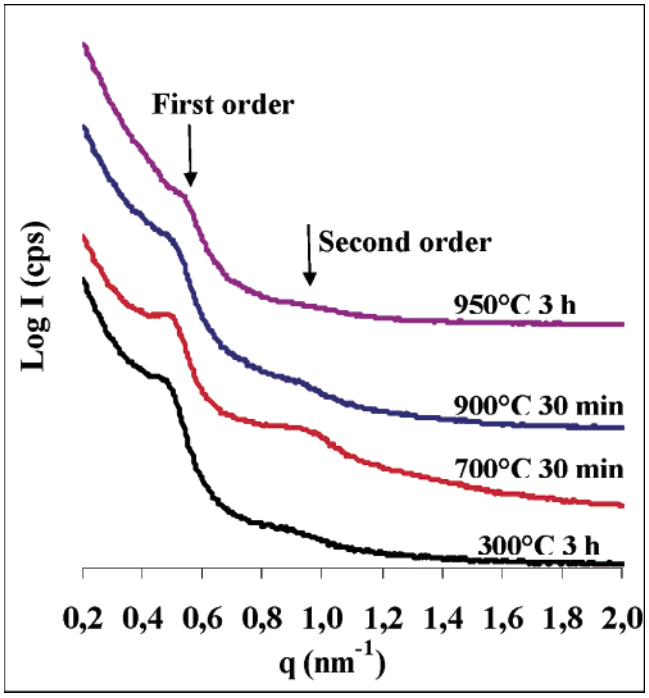

Figure 2. SAXS diagrams of powder calcined in air at various temperatures with a ramp of 5 °C·min^{-1} after 500 °C. Two orders of diffraction are visible on each diagram, suggesting a high degree of ordering and high stability upon thermal treatment.

average diameter of 13 nm. Layers of spherical pores are lying along the particle/air curved interface and stack one to the other into a compact 3D structure (see hexagon inset Figure 1a). The organization becomes difficult to assess at the particle center as a result of a higher quantity of matter that electrons have to cross before reaching the microscope screen. However, smaller particles reveal a similar structure within their body as seen in Figure 1 (bottom left). Arrangement of pores is similar in both cases except that some particles seem to have collapsed after 30 min at 900 °C. The long-range well-ordered mesostructure is confirmed by the SAXS diagrams in Figure 2, where an intense Bragg peak is present at low angle for each case. The second-order peak, confirming the high degree of ordering, is also clearly discernible but decreases in intensity after 900 °C, suggesting that the overall mesostructure is just slightly deteriorated upon thermal treatment. The corresponding *d*-spacing is 15 nm at 300 °C and is reduced to 14 nm at 900 °C, which is attributed to a slight lattice contraction induced by the dehydration and condensation of the alumina network. The intensity of the peaks increases between 300 and 700 °C as a result of the increase in electron density contrast due to the decomposition and elimination of the copolymer hydrophobic parts located inside the pores and the progressive densification of the network. These peaks cannot be attributed to a specific phase as a result of the high curvature imposed by the particles surface with respect to the lattice parameter. Indeed, extension of the ordered domains applies at the curved spherical interface, which prevents construction of all Bragg signals for such structure. On the other hand, TEM images (Figure 1) give a good idea of the high degree of pore local ordering into a tridimensional network.

The powder porosity was investigated by N_2-adsorption/desorption at 77 K (see Figure 3). After 30 min at 700 °C in air, alumina powders present an isotherm (a) characteristic of mesoporous materials with a hysteresis loop of type IV. The BET surface area was 403 m^2·g^{-1}, while the pore volume, estimated from the total volume of N_2 uptake just above capillary condensation, was 0.56 cm^3·g^{-1}. The sharp uptake in the nitrogen adsorption branch confirms the presence of pores with diameter centered at 13 nm, as determined according to the Broekhoff-Deboer algorithm (see pore size distribution (b)). This value is in agreement with TEM and SAXS data. The desorption branch shows a progressive evaporation of liquid nitrogen and terminates at around $P/P_0 = 0.42$, which is the critical pressure of instability of the liquid nitrogen meniscus. Precise determination of pore window dimension is thus impossible, but one can safely state that pores are highly accessible through interconnections of various dimensions. After 30 min at 900 °C, the network reveals adsorption−desorption behavior similar to the preceding network (similar isotherm shape) except that the pore volume and surface area were reduced to 0.34 cm^3·g^{-1} and 134 m^2·g^{-1}, respectively, as a result of the network modification also observed by TEM and

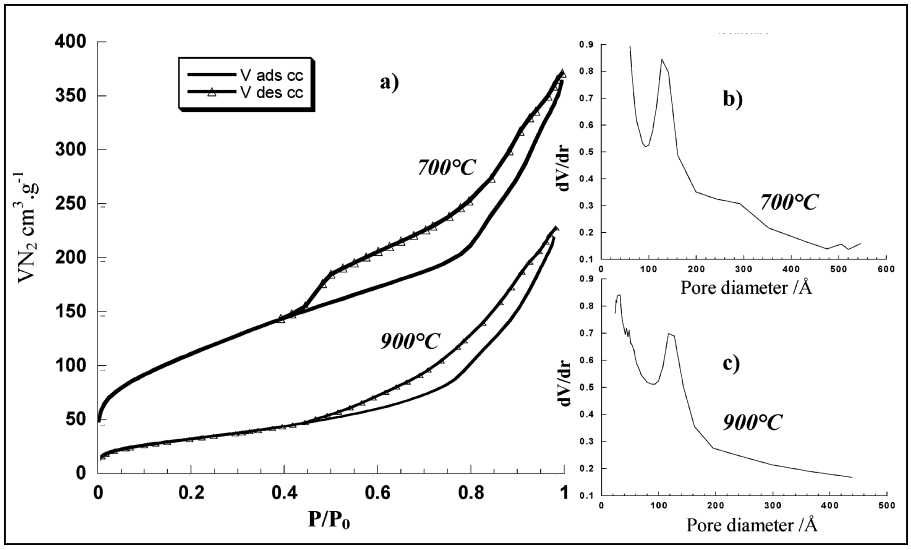

Figure 3. N_2-BET isotherm (a) and corresponding pore size distribution (b) and (c) of powders calcined 30 min at 700 °C and 30 min at 900 °C.

SAXS. The structure remains well-ordered and mesoporous with a pore size distribution centered at 12.5 nm (adsorption Figure 1c) and a large distribution of interconnection windows. In both cases, the uptake recorded at higher pressures is attributed to interparticle porosity and has a high contribution as a result of the small size of the spherical primary particles (see TEM image Figure 1b). T-plot analyses (where the adsorbed volume of N_2 is plotted versus the layer thickness of N_2 adsorbed on a flat surface at P/P_0) shows that, at 700 °C, 30% of the mesoporous volume is attributed to small mesopores with average pore diameter of 3 nm, while the 70% remaining is due to the larger mesopores with average diameter of 12.5 nm. These smaller mesopores correspond to the porosity existing between Al_2O_3 particles (≈6 nm in diameter, see XRD data) composing the framework. At 900 °C, the contribution of the small mesopores decreases to approximately 10% of the mesoporous volume as a result of densification of the framework. Insignificant contribution of micropores was deduced for both temperatures of treatment. The high porous volume and surface area are thus attributed to the combination of aerosol particles of small dimensions with an internal well-calibrated mesoporosity and residual nanobuilding blocks interparticle porosity.

Figure 4 represents wide angle XRD diagrams of mesoporous alumina powder samples treated 10 and 30 min at 900 °C, and at 950 °C for 2 h. One observes that crystallization of the network takes place between 10 and 30 min at 900 °C since no diffraction peaks were recorded before this period at 900 °C. The peak indexation is characteristic of the γ-alumina phase (*Fd3m* lacunar spinel), even if fluctuations are often encountered in the indexation of the latter phase.[41−43] Applying the Scherer equation to the (400) and the (440) peaks, we calculated a maximal particle size of 6 nm. This particle size is in agreement with the dimension of the pore (13 nm) and the mesostructure *d*-spacing

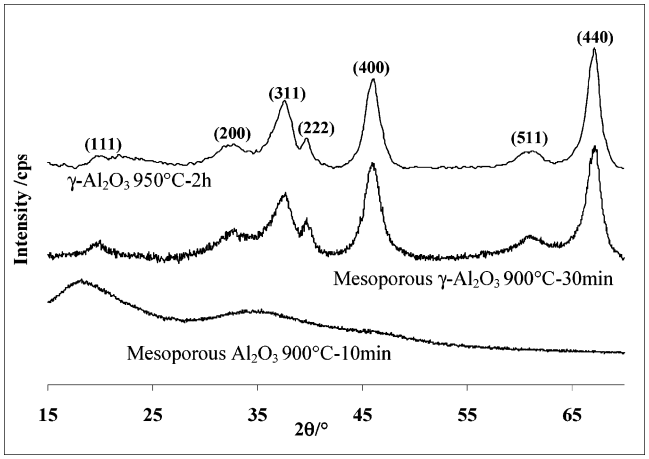

Figure 4. XRD analysis of powders calcined at various temperatures showing that crystallization into γ-Al_2O_3 phase is achieved between 10 and 30 min at 900 °C following the thermal treatment history described in the Experimental Section.

(14 nm). Assuming a hexagonal arrangement of pores (see Figure 1), the distance between two adjacent pores is $d^*\sqrt{2} \approx 20.5$ nm and since pores are 13 nm in diameter, they are separated by around 7.5 nm of alumina walls. Since the γ-Al_2O_3 phase is reported to be full of defects (oxygen and Al^{3+} vacancies randomly distributed within the spinel lattice), we performed a ^{27}Al NMR spectroscopic study to follow the evolution of the Al^{3+} local atomic environments with the thermal treatment. The ^{27}Al MAS NMR spectra (Figure 5a) of the samples treated at various temperatures show three asymmetric lines having maxima at 63, 32, and 5 ppm. According to the literature,[44] these bands are assigned to the central $<-1/2,1/2>$ transition of the Al^{3+} ion in 4-fold (AlO_4), 5-fold (AlO_5), and 6-fold (AlO_6) coordination, respectively. The spectra were deconvoluted (Figure 5C) using the Dmfit program[45] for quantitative analysis (Figure 5b): the observed

(41) Krokidis, X.; Raybaud, P.; Gobichon, A. E.; Rebours, B.; Euzen, P.; Toulhoat, H. *J. Phys. Chem. B* **2001**, *105*, 5121.
(42) Digne, M.; Sautet, P.; Raybaud, P.; Euzen, P.; Toulhoat, H. *J. Catal.* **2004**, *211*, 1.
(43) Digne, M.; Sautet, P.; Raybaud, P.; Euzen, P.; Toulhoat, H. *J. Catal.* **2004**, *226*, 54.
(44) Stebbins, J. F. Nuclear magnetic resonance spectroscopy of silicates and oxides ingeochemistry and geophysics. In *Handbook of Physical Constants, v. 2*; Ahrens, T. J., Ed.; American Geophysical Union: Washington DC, 1995.
(45) Massiot, D.; Fayon, F.; Capron, M.; King, I.; Le Calvé, S.; Alonso, B.; Durand, J.-O.; Bujoli, B.; Gan, Z.; Hoatson, G. *Magn. Reson. Chem.* **2002**, *40*, 70.

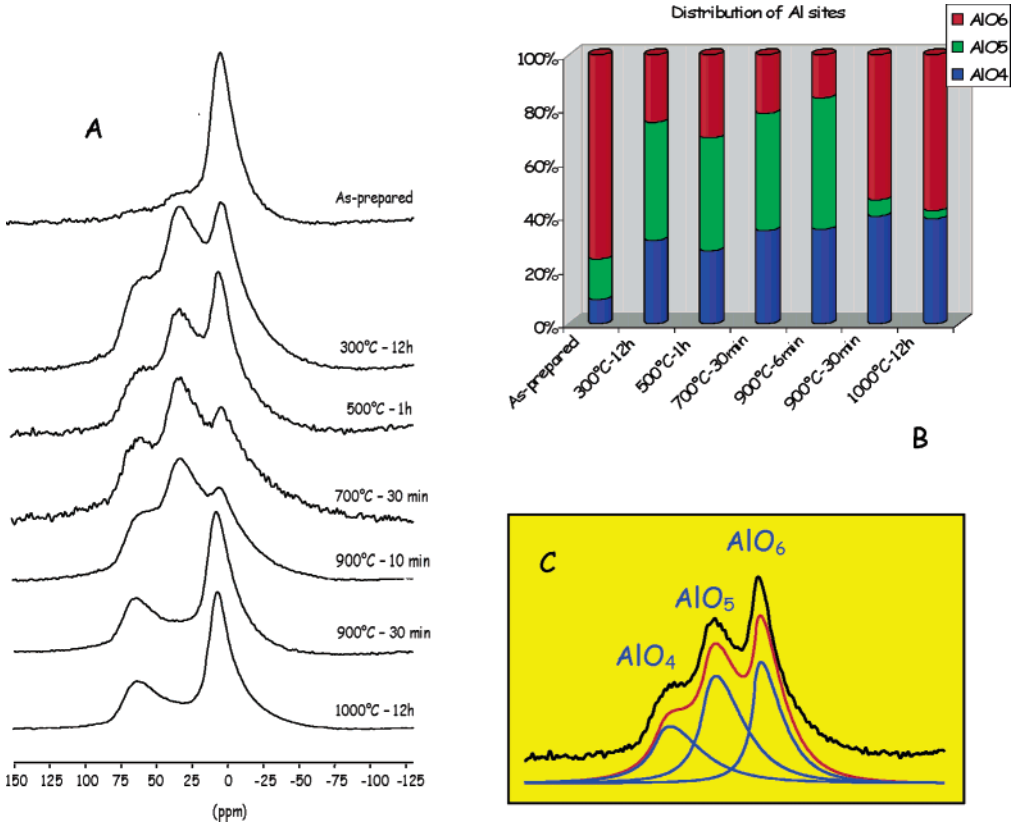

Figure 5. ^{27}Al MAS NMR studies of the evolution of aluminum center chemical environment versus temperature of treatment: (A) spectra, (B) distribution of Al^{3+} sites, and (C) example of spectrum simulation.

asymmetric line shape reflects a distribution of isotropic chemical shifts, asymmetry parameter, and quadrupolar couplings, which was simulated with an already published simple model.[18,46] One notices that the as-prepared (uncalcined) powder is mainly composed of hexacoordinated Al^{3+}, which is likely to correspond to the AlOOH boehmite intermediate phase. This latter sample did not show the typical XRD signature of the lamellar phase expected for boehmite (Figure 4), as a result of the combination of the confinement of the domains within the nanometric walls and the perturbation created by the presence of the PEO chains encrusted into them. This latter interpenetration was reported for Pluronic-templated SiO_2 materials[47] and is likely to occur in the present case as a result of the high hydrophilicity of the hydrated alumina interacting with the PEO chains of the copolymer template. Along the thermal treatment and up to 900 °C-10 min, Al^{3+} ions are distributed between the three sites of coordination with a higher proportion of AlO_5 (44−50%), which is attributed to the high quantity of defects created by the large surface area of the network. Before crystallization, proportions of AlO_4 and AlO_5 have a global tendency to increase with temperature, which is consistent with the dehydration. Crystallization occurs between 10 and 30 min at 900 °C and is clearly accompanied by the sudden drop of AlO_5 population on account of an increase of AlO_6 sites. The number of AlO_4 sites does not vary significantly and remains between 35 and 40%. After crystallization, mainly AlO_6 and AlO_4 sites are thus observed, which is characteristic of the γ-alumina phase. The expected maximal value of ≈40% (AlO_4) and ≈60% of (AlO_6) of the γ-phase is also verified. Therefore, a similar proportion of AlO_4 is likely to stand at the material surface before and after crystallization. The presence of a few percent of AlO_5 species can be attributed to surface cationic centers. Samples were treated for 12 h at 1000 °C to extend the crystallization by sintering. Such samples exhibit the same NMR spectra than that recorded after 30 min at 900 °C, which suggests that, after 30 min at 900 °C, the network contains at worst an undetectable proportion of amorphous domains and is mainly composed of γ-Al_2O_3 nanocrystalline particles. Powders that have been treated longer than 30 min at 900 °C or at higher temperature than 900 °C present less defined long-range ordered peaks by SAXS (Figure 2), better defined XRD peaks (Figure 4), and larger than 50 nm in size crystalline particles by TEM (see Supporting Information SI1), while the structure is still characteristic of the γ-alumina phase. One can safely state that the mesostructured network started to collapse above 30 min at 900 °C, leading to the formation of larger sintered crystals. However, it is of utmost importance to underline that, after 700 °C and before crystallization at 900 °C (longer than 10 min), the network is mainly formed of AlO_4 and AlO_5 sites which are the acidic centers making alumina-based mesoporous networks interesting for high-temperature heterogeneous catalysis processes. Designing a whole set of mesoporous catalytic supports is thus possible by adjusting ceramization conditions between 700 and 900 °C.

(46) Neuville, D. R.; Cormier, L.; Massiot, D. *Geochim. Cosmochim. Acta* **2004**, *68*, 5071.
(47) Melosh, N. A.; Lipic, P.; Bates, F. S.; Wudl, F.; Stucky, G. D.; Fredrickson, G. H.; Chmalka, B. F. *Macromolecules* **1999**, *32*, 4332.

It is well-known that crystalline transition alumina phases are formed through a complicated sequence of phase transition from hydrated hydroxide (gibbsite) and oxyhydroxide (boehmite) to the thermodynamically stable α-Al_2O_3. At moderate temperature, several metastable "transition" oxide phases can be formed and the γ-Al_2O_3 one is usually encountered as the first crystalline phase formed by dehydration of AlOOH around 500 °C.[48] This dehydration step is usually accompanied by the collapsing of the meso-order.[22] Such a deterioration is avoided here as a result of the thermal stability of the hydrophobic part of the template that remains confined within the nanocavity (mesopores) during dehydration and up to its thermal degradation above 350 °C. Such stabilization is well-described for thin film systems.[9] Actual mesoporosity is thus achieved above 400 °C. In the presence of a porous mesostructure, no crystalline phase was observed by XRD below 10 min at 900 °C. The stabilization of such an amorphous state up to 900 °C has to be related to the high surface area of the amorphous intermediate[49] but seems to be enhanced by the ordered mesostructure. Indeed, the inorganic walls of the as-prepared materials (below 300 °C) are formed of amorphous small clusters of hexacoordinated Al^{3+} that are stabilized by hydrogen bonding with the highly hydrophilic interpenetrating PEO chains. Upon PEO thermal decomposition and inorganic dehydration, part of the initial population of hexacoordinated Al^{3+} adopts either penta- or tetracoordination. The highest proportion of pentacoordinated Al^{3+} is reached at 700 °C, and no change is noticed (see ^{27}Al NMR spectra) before crystallization into γ-Al_2O_3. This outstanding proportion of pentacoordinated Al^{3+} cations, associated with the confinement of the matter within the nanoscopic wall edifices, is likely to be responsible for the stabilization of the amorphous oxide phase at such high temperatures. In addition, since the γ-Al_2O_3 phase results of the dehydration-driven collapsing of the boehmite oxyhydroxide layers (topotactic transformation), having no boehmite structure at moderate temperatures (see XRD) prevents easy crystallization before 900 °C-10 min. Once nucleation took place, one observes that γ-Al_2O_3 domains have grown to a metastable limited size of 6 nm. These nanoparticles can be stabilized within such an edifice as the results of confinement imposed by the pore interface because of the homogeneous small wall dimension related to the ordered mesostructure, because of the consequent high surface energy contribution versus bulk energy, and finally because of the intrinsic high vacancy content of the spinel γ-Al_2O_3 structure, already limiting the kinetics of particle growth. However, ^{27}Al NMR studies showed that most of the Al^{3+} is located in AlO_4 and AlO_6 sites, suggesting that most of the matter is under crystalline form and that these nanodomains are homogeneous. Forcing the domains to sinter at 950 °C for 2 h or at 1000 °C for 12 h led to larger crystallites and collapsing of the mesoporosity, but no significant aluminum atomic local variation is noticed by NMR when compared to the previous 900 °C-30 min treated nanocrystalline sample. In summary, the sequential events occurring during thermal treatment is dehydration, organic decomposition, nucleation, and limited growth of γ-Al_2O_3 particles up to the interface, to finish by extended sintering. Stabilization of a pure nanocrystalline mesoporous network at high temperature is thus attributed to the controlled use of stable polymers allowing dehydration in the presence of polymer nanodomains, the control of the treatment conditions, the intrinsic lacunar state of the microstructure, and the high order and high surface area characteristic of a surfactant-templated mesoporous network.

Conclusion

In summary, we reported the first crystalline (γ-Al_2O_3) ordered mesoporous UPMC1 powder stable at a temperature as high as 900 °C. This was elaborated by evaporation-induced self-assembly, associated with aerosol generation, followed by careful thermal treatment. Such controlled thermal treatments allow designing of an entire set of mesoporous catalytic supports by adjusting ceramization conditions between 700 and 900 °C. In addition to the potential interest of such crystalline and/or amorphous materials in catalysis and separation due to its highest content in acidic AlO_4 and AlO_5 sites, the present work highlights the stabilization of ordered amorphous and/or metastable nanocrystalline frameworks at very high temperatures, induced by the high porosity and surface area and by the ordered mesoporosity imposed by the network they composed. The intrinsic physicochemical properties of highly stable alumina combined with high surface area makes these UPMC1 materials ideal candidates for heterogeneous catalysis. It also opens novel perspectives of a way toward the elaboration of other types of interesting mesoporous crystalline powders such as intrinsic semiconducting TiO_2 or SnO_2.

Acknowledgment. The authors would like to thank the European Network of Excellence FAME and the CNRS. The Centre of Electronic Microscopy of Orléans (France) is acknowledged for the TEM analyses. We also acknowledge the help of Jocelyne Maquet with NMR experiments.

Supporting Information Available: TEM image of alumina mesoporous powder. This material is available free of charge via the Internet at http://pubs.acs.org.

CM061489J

(48) Pecharroman, C.; Sobrados, I.; Iglesias, J. E.; Gonzales-Carreno, T.; Sanz, J. *J. Phys. Chem. B* **1999**, *103*, 6160.
(49) Castro, R. H. R.; Ushakov, S. V.; Gemgembre, L.; Gouvea, D.; Navrotsky, A. *Chem. Mater.* **2006**, *18*, 1867.